Table S1. List of background NOAA stations used in this study for assimilation and comparison.

ID	Location	Latitude	Longitude	Alt. [m]
ALT	Alert, Nunavut, Canada	82.45°N	62.51°W	185.0
ZEP	Ny-Ålesund, Svalbard, Norway and Sweden	78.91°N	11.89°E	474.0
SUM	Summit, Greenland	72.60°N	38.42°W	3209.5
BRW	Barrow, Alaska, United States	71.32°N	156.61°W	11.0
PAL	Pallas-Sammaltunturi, Finland	67.97°N	24.12°E	565.0
ICE	Storhofdi, Vestmannaeyjar, Iceland	63.40°N	20.29°W	118.0
CBA	Cold Bay, Alaska, United States	55.21°N	162.72°W	21.3
MHD	Mace Head, County Galway, Ireland	53.33°N	9.90°W	5.0
SHM	Shemya Island, Alaska, United States	52.71°N	174.13°E	23.0
UUM	Ulaan Uul, Mongolia	44.45°N	111.10°E	1007.0
NWR	Niwot Ridge, Colorado, United States	40.05°N	105.59°W	3523.0
UTA	Wendover, Utah, United States	39.90°N	113.72°W	1327.0
AZR	Terceira Island, Azores, Portugal	38.77°N	27.38°W	19.0
WLG	Mt. Waliguan, Peoples Republic of China	36.29°N	100.90°E	3810.0
LMP	Lampedusa, Italy	35.52°N	12.63°E	45.0
BMW	Tudor Hill, Bermuda, United Kingdom	32.27°N	64.88°W	30.0
IZO	Izana, Tenerife, Canary Islands, Spain	28.31°N	16.50°W	2372.9
MID	Sand Island, Midway, United States	28.22°N	177.37°W	4.6
ASK	Assekrem, Algeria	23.26°N	5.63°E	2710.0
KUM	Cape Kumukahi, Hawaii, United States	19.56°N	154.89°W	8.0
MLO	Mauna Loa, Hawaii, United States	19.54°N	155.58°W	3397.0
MEX	Sierra Negra Volcano, Mexico	18.98°N	97.31°W	4464.0
GMI	Mariana Islands, Guam	13.39°S	144.66°E	0.0
RPB	Ragged Point, Barbados	13.17°N	59.43°W	15.0
CHR	Christmas Island	1.70°N	157.15°W	0.0
SEY	Mahe Island, Seychelles	4.68°S	55.53°E	2.0
NAT	Farol De Mae Luiza, Brazil	5.80°S	35.19°W	50.0
ASC	Ascension Island, United Kingdom	7.97°S	14.40°W	85.0
SMO	Tutuila, American Samoa	14.25°S	170.56°W	42.0
NMB	Gobabeb, Namibia	23.58°S	15.03°E	456.0
EIC	Rapa Nui, Chile	27.16°S	109.43°W	47.0
CPT	Cape Point, South Africa	34.35°S	18.49°E	230.0
CGO	Cape Grim, Tasmania	40.68°S	144.69°E	94.0
BHD	Baring Head Station, New Zealand	41.41°S	174.87°E	85.0
CRZ	Crozet Island, France	46.43°S	51.85°E	197.0
USH	Ushuaia, Argentina	54.85°S	68.31°W	12.0
PSA	Palmer Station, Antarctica, United States	64.77°S	64.05°W	10.0
SYO	Syowa Station, Antarctica, Japan	69.01°S	39.59°E	14.0
SPO	South Pole, Antarctica, United States	89.98°S	24.80°W	2810.0

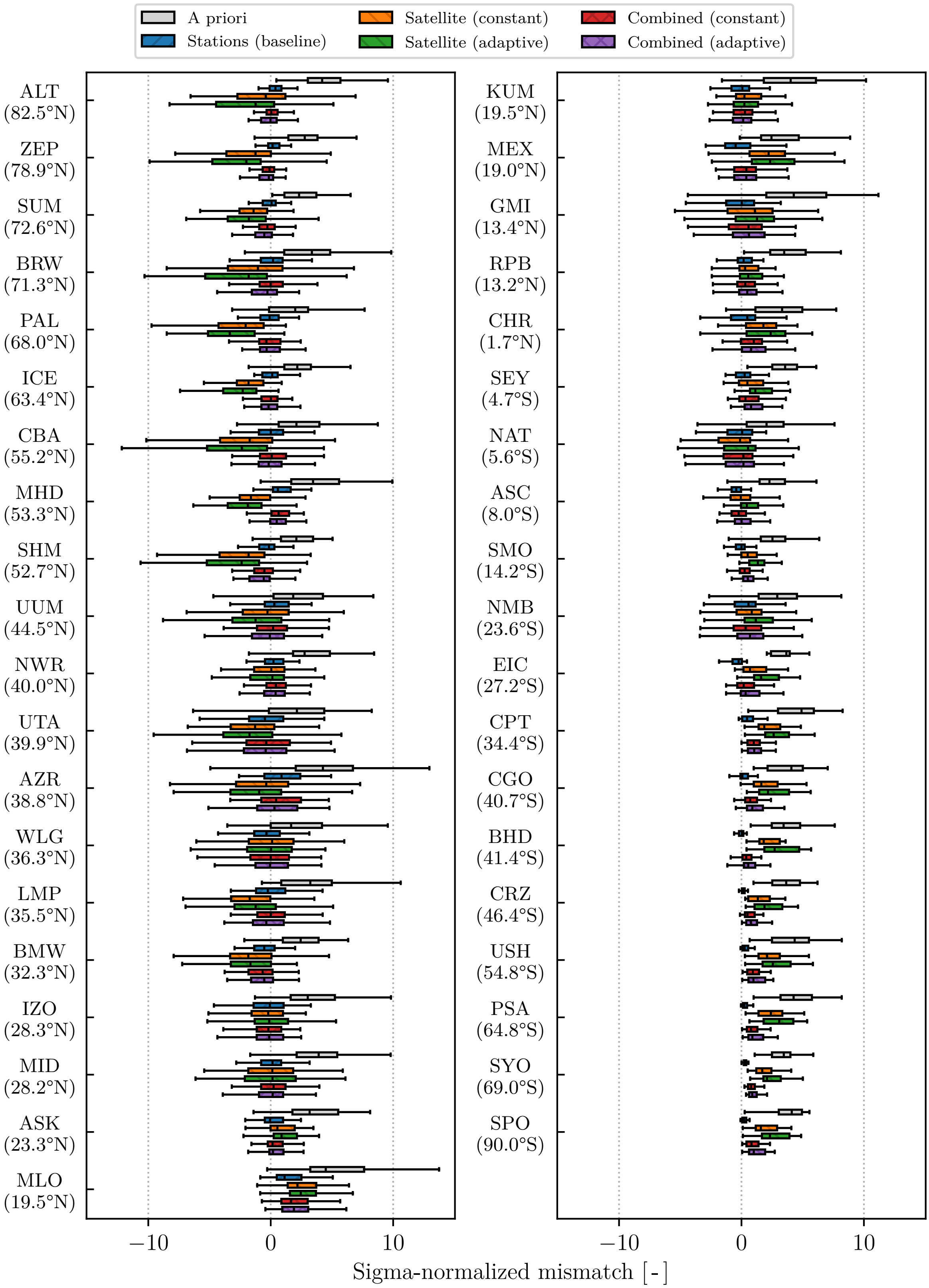

Figure S1. Comparison of the sigma-normalized mismatch between posterior model output and NOAA flask measurements. All selected background stations with available data for the simulation period are shown.

Table S2. List of TCCON sites used in this study for comparison and validation.

ID	Location	Lat.	Lon.	Alt. [m]	Data Citation
EU	Eureka, Canada	80.05°N	86.42°W	610.0	Strong et al. (2022)
NY	Ny-Ålesund, Svalbard	78.90°N	11.90°E	20.0	Buschmann et al. (2022)
SO	Sodankylä, Finland	67.37°N	26.63°E	188.0	Kivi et al. (2022)
ET	East Trout Lake, Canada	54.35°N	104.99°W	502.0	Wunch et al. (2022)
BR	Bremen, Germany	53.10°N	8.85°E	27.0	Notholt et al. (2022)
KA	Karlsruhe, Germany	49.10°N	8.44°E	116.0	Hase et al. (2024)
PR	Paris, France	48.85°N	2.36°E	60.0	Té et al. (2022)
OR	Orleans, France	47.97°N	2.11°E	130.0	Warneke et al. (2024)
GM	Garmisch, Germany	47.48°N	11.06°E	740.0	Sussmann and Rettinger (2023)
PA	Park Falls, Wisconsin, USA	45.95°N	90.27°W	440.0	Wennberg et al. (2022b)
RJ	Rikubetsu, Hokkaido, Japan	43.46°N	143.77°E	380.0	Morino et al. (2022a)
XH	Xianghe, China	39.80°N	116.96°E	36.0	Zhou et al. (2022)
OC	Lamont, Oklahoma, USA	36.60°N	97.49°W	320.0	Wennberg et al. (2022c)
TK	Tsukuba, Ibaraki, Japan	36.05°N	140.12°E	30.0	Morino et al. (2022b)
NI	Nicosia, Cyprus	35.14°N	33.38°E	185.0	Petri et al. (2024)
DF	Edwards, California, USA	34.96°N	117.88°W	699.0	Iraci et al. (2022)
CI	Pasadena, California, USA	34.14°N	118.13°W	230.0	Wennberg et al. (2022a)
JS	Saga, Japan	33.24°N	130.29°E	7.0	Shiomi et al. (2022)
HF	Hefei, China	31.91°N	117.17°E	29.0	Liu et al. (2023)
IZ	Izana, Tenerife, Spain	28.30°N	16.50°W	2,370.0	García et al. (2022)
BU	Burgos, Philippines	18.53°N	120.65°E	35.0	Morino et al. (2022c)
DB	Darwin, Australia	12.42°S	130.89°E	3.0	Deutscher et al. (2023b)
RA	Reunion Island, France	20.90°S	55.49°E	87.0	De Mazière et al. (2022)
WG	Wollongong, Australia	34.41°S	150.88°E	30.0	Deutscher et al. (2023a)
LR	Lauder, New Zealand	45.04°S	169.68°E	370.0	Pollard et al. (2022)

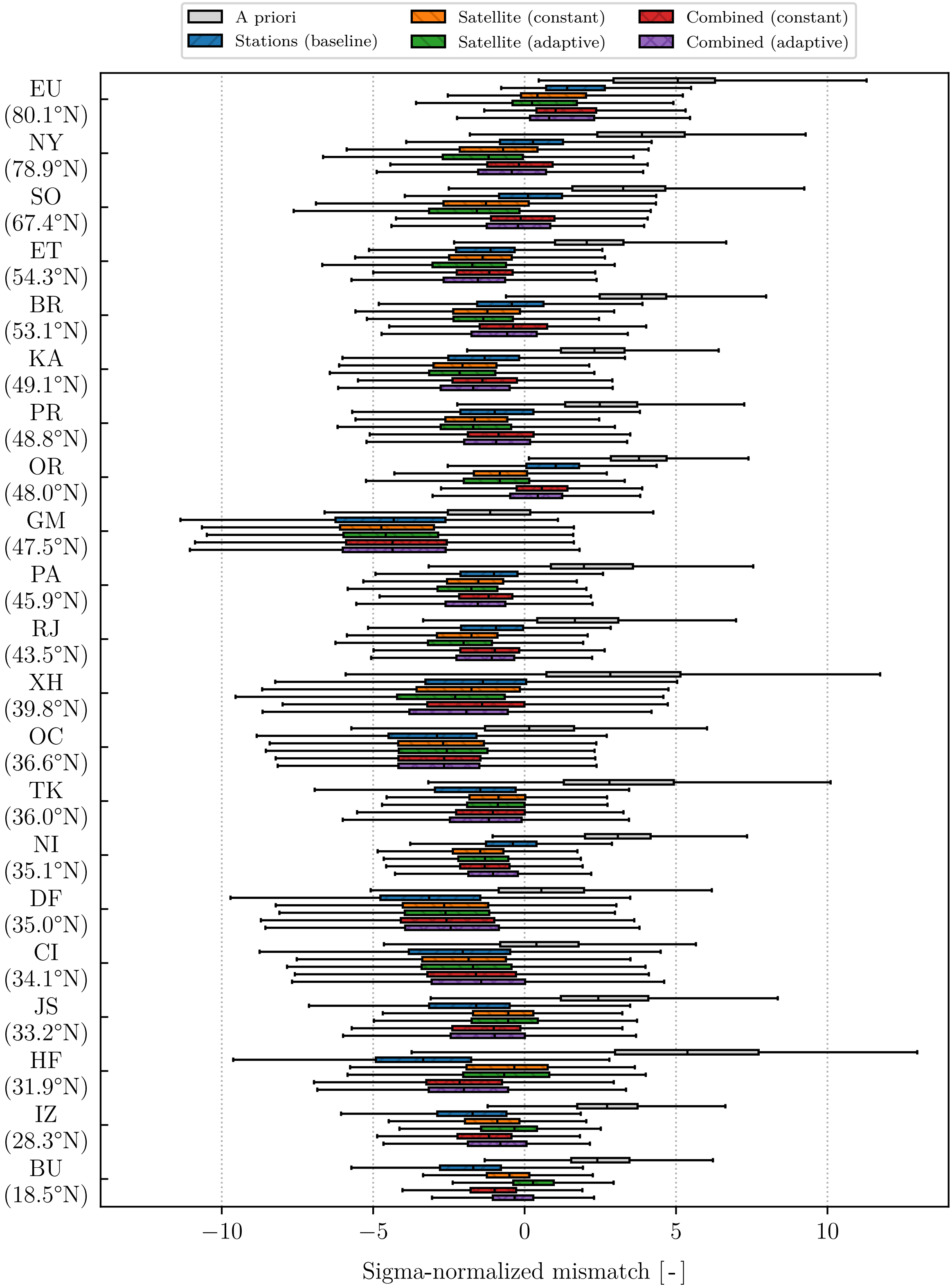

Figure S2. Comparison of the sigma-normalized mismatch between posterior model output and TCCON observations. Sites are sorted by latitude. Showing Northern Hemisphere sites.

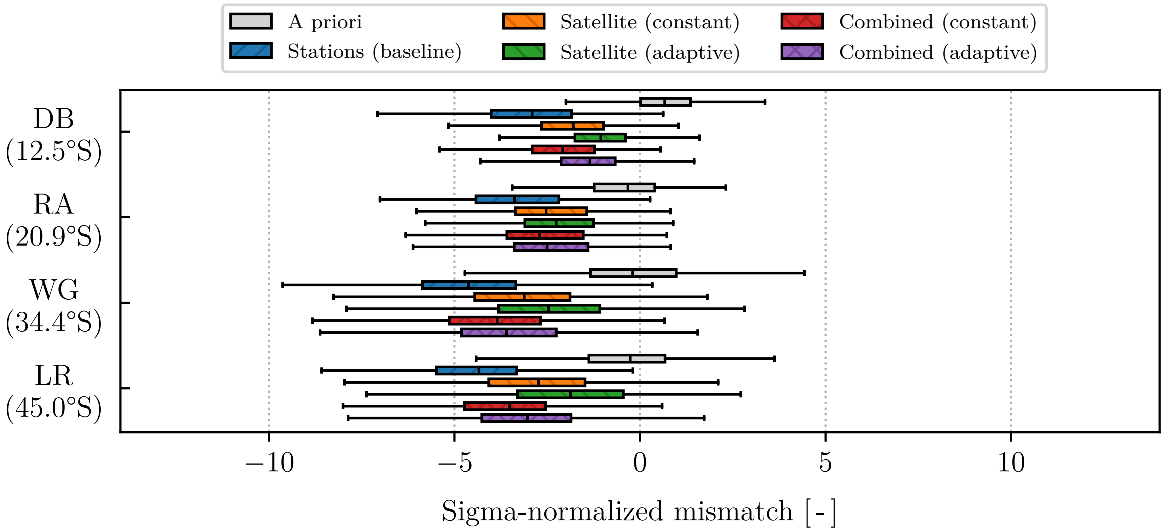

Figure S2. (Continued) Comparison of the sigma-normalized mismatch between posterior model output and TCCON observations. Sites are sorted by latitude. Showing Southern Hemisphere sites.

Table S3. Summary of statistical metrics of modeled results against TCCON observations. Both RMSE and MBE are reported in ppb, and mismatch in unitless deviations from sigma.

Sim	Weighted RMSE	Weighted MBE	Normalized mismatch
EU (80.05°N) $n = 1,337$			
S0	19.30	18.73	4.86
S1	8.61	7.01	1.84
S2	7.99	4.35	1.14
S3	7.50	3.24	0.86
S4	8.24	6.01	1.58
S5	7.88	5.21	1.37
NY (78.92°N) $n = 2,016$			
S0	13.89	12.71	3.84
S1	4.84	0.85	0.24
S2	7.14	-2.92	-0.90
S3	8.77	-4.92	-1.50
S4	5.30	-0.54	-0.18
S5	5.77	-1.39	-0.43
SO (67.37°N) $n = 3,302$			
S0	12.47	10.76	3.16
S1	5.59	0.51	0.12
S2	8.84	-4.57	-1.40
S3	10.34	-6.11	-1.86
S4	5.93	-0.44	-0.17
S5	6.12	-0.91	-0.31
ET (54.35°N) $n = 5,131$			
S0	10.07	8.22	2.22
S1	7.18	-5.03	-1.30
S2	8.20	-5.82	-1.56
S3	9.81	-7.20	-1.94
S4	7.06	-5.14	-1.36
S5	8.40	-6.58	-1.76
BR (53.1°N) $n = 317$			
S0	12.12	10.84	3.56
S1	5.80	-1.46	-0.47
S2	6.47	-3.88	-1.27
S3	7.11	-4.50	-1.47
S4	5.10	-1.04	-0.33
S5	5.26	-1.88	-0.61

Sim	Weighted RMSE	Weighted MBE	Normalized mismatch
KA (49.1°N) $n = 2,711$			
S0	8.96	7.21	2.28
S1	6.97	-4.42	-1.39
S2	7.92	-6.03	-1.91
S3	8.42	-6.36	-2.02
S4	6.66	-4.30	-1.36
S5	7.37	-5.26	-1.67
PR (48.85°N) $n = 1,401$			
S0	9.79	7.69	2.48
S1	6.95	-3.29	-1.04
S2	7.59	-5.19	-1.67
S3	7.78	-5.10	-1.64
S4	6.34	-2.89	-0.92
S5	6.60	-3.23	-1.03
OR (47.96°N) $n = 2,203$			
S0	12.67	11.98	3.78
S1	5.53	2.97	0.95
S2	5.27	-2.53	-0.80
S3	6.17	-2.87	-0.91
S4	4.51	1.86	0.59
S5	4.55	1.23	0.40
GM (47.48°N) $n = 2,419$			
S0	8.29	-3.83	-1.16
S1	16.56	-14.94	-4.57
S2	17.09	-15.65	-4.79
S3	16.93	-15.28	-4.68
S4	16.24	-14.64	-4.47
S5	16.57	-14.84	-4.54
PA (45.94°N) $n = 5,078$			
S0	10.94	8.89	2.20
S1	7.17	-4.89	-1.20
S2	8.38	-6.65	-1.71
S3	9.31	-7.66	-1.96
S4	7.21	-5.33	-1.35
S5	8.38	-6.69	-1.70

Table S3. (continued)

Sim	Weighted RMSE	Weighted MBE	Normalized mismatch
RJ (43.46°N) $n = 989$			
S0	9.83	7.30	1.86
S1	7.19	-4.22	-1.11
S2	8.79	-7.31	-1.94
S3	9.72	-8.28	-2.19
S4	6.96	-4.55	-1.20
S5	7.56	-5.37	-1.41
XH (39.8°N) $n = 3,647$			
S0	17.38	11.11	3.10
S1	12.70	-5.87	-1.75
S2	13.15	-7.35	-2.04
S3	14.50	-9.49	-2.63
S4	12.52	-5.77	-1.69
S5	13.70	-8.14	-2.33
OC (36.6°N) $n = 7,012$			
S0	9.21	-0.19	-0.07
S1	14.31	-12.11	-3.26
S2	13.88	-11.26	-3.02
S3	13.71	-10.95	-2.94
S4	13.57	-11.31	-3.05
S5	13.74	-11.41	-3.07
TK (36.05°N) $n = 1,397$			
S0	13.15	10.55	3.13
S1	8.22	-5.46	-1.64
S2	5.75	-3.07	-0.92
S3	5.72	-3.08	-0.93
S4	6.83	-3.95	-1.19
S5	7.21	-4.48	-1.35
NI (35.14°N) $n = 2,224$			
S0	12.36	10.84	3.17
S1	5.16	-1.69	-0.50
S2	7.17	-5.38	-1.55
S3	6.77	-4.82	-1.38
S4	6.55	-4.64	-1.34
S5	6.01	-3.75	-1.08

Sim	Weighted RMSE	Weighted MBE	Normalized mismatch
DF (34.96°N) $n = 9,727$			
S0	6.92	1.61	0.51
S1	12.48	-9.78	-3.11
S2	10.64	-8.37	-2.66
S3	10.52	-8.24	-2.62
S4	10.80	-8.06	-2.57
S5	10.45	-7.56	-2.41
CI (34.14°N) $n = 5,031$			
S0	6.83	1.43	0.43
S1	11.03	-6.97	-2.16
S2	10.19	-6.66	-2.07
S3	10.09	-6.43	-2.00
S4	9.78	-5.61	-1.74
S5	9.66	-4.97	-1.55
JS (33.24°N) $n = 2,173$			
S0	13.78	11.31	2.86
S1	9.86	-6.88	-1.76
S2	6.42	-2.75	-0.70
S3	7.27	-2.39	-0.61
S4	7.92	-4.70	-1.19
S5	8.25	-4.34	-1.11
HF (31.9°N) $n = 343$			
S0	20.57	16.92	5.08
S1	13.90	-10.51	-3.41
S2	7.58	-2.13	-0.74
S3	7.74	-2.25	-0.77
S4	10.43	-6.72	-2.21
S5	10.00	-6.16	-2.02
IZ (28.31°N) $n = 1,907$			
S0	9.38	8.28	2.76
S1	7.10	-5.33	-1.77
S2	5.16	-3.16	-1.05
S3	4.38	-1.53	-0.50
S4	5.67	-4.07	-1.35
S5	5.03	-2.86	-0.95

Table S3. (continued)

Sim	Weighted RMSE	Weighted MBE	Normalized mismatch
BU (18.53°N) $n = 3,732$			
S0	11.28	10.49	2.54
S1	9.18	-8.17	-1.84
S2	5.35	-2.74	-0.57
S3	4.59	0.77	0.27
S4	6.47	-5.09	-1.13
S5	4.81	-2.19	-0.42
DB (12.46°S) $n = 3,197$			
S0	4.51	2.45	0.69
S1	11.43	-10.81	-2.95
S2	7.92	-7.00	-1.91
S3	5.54	-4.16	-1.14
S4	8.69	-7.91	-2.16
S5	6.48	-5.33	-1.46
RA (20.9°S) $n = 1,305$			
S0	5.12	-2.04	-0.40
S1	15.82	-15.36	-3.35
S2	12.15	-11.53	-2.48
S3	11.01	-10.34	-2.23
S4	12.75	-12.18	-2.62
S5	11.99	-11.38	-2.45
WG (34.41°S) $n = 3,785$			
S0	5.91	-0.73	-0.25
S1	16.08	-14.96	-4.72
S2	11.86	-10.30	-3.25
S3	10.25	-8.01	-2.54
S4	13.91	-12.65	-3.99
S5	13.09	-11.61	-3.67
LR (45.04°S) $n = 5,233$			
S0	4.74	-1.12	-0.36
S1	14.56	-13.85	-4.41
S2	10.35	-8.87	-2.82
S3	8.54	-6.13	-1.95
S4	12.34	-11.45	-3.64
S5	11.07	-9.82	-3.12

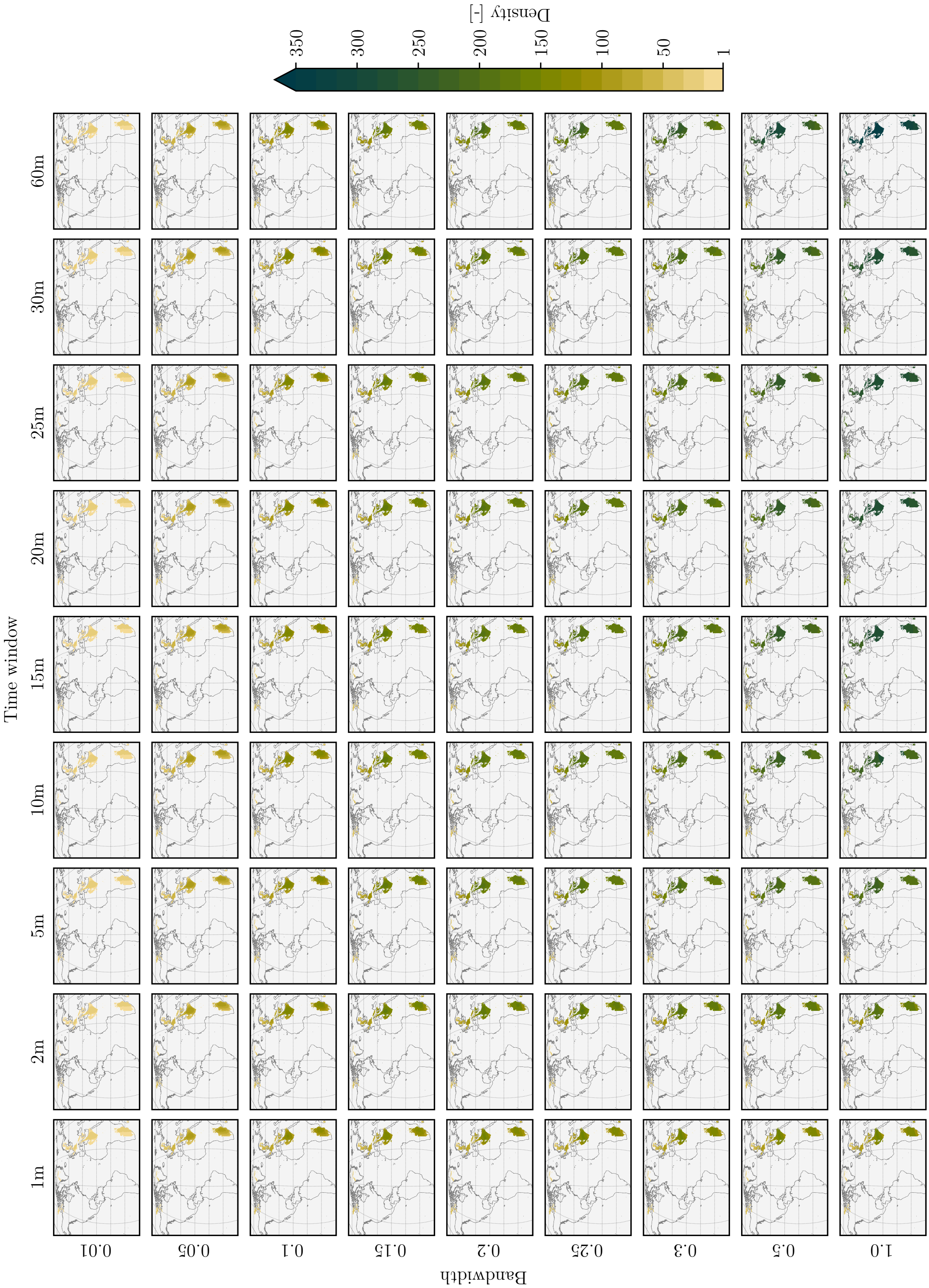

Figure S3. Sensitivity test of the Kernel Density Estimation for the bandwidth h, and the time window. Results are for orbit 3,718 (2018-07-02). Note that the time window is defined as the domain to calculate densities, but an extra neighborhood of the same time-length is included both backwards and forward. A time window of 60 minutes already starts considering points that are spatially close, but far enough in time (i.e., in different orbits) to be invalid.

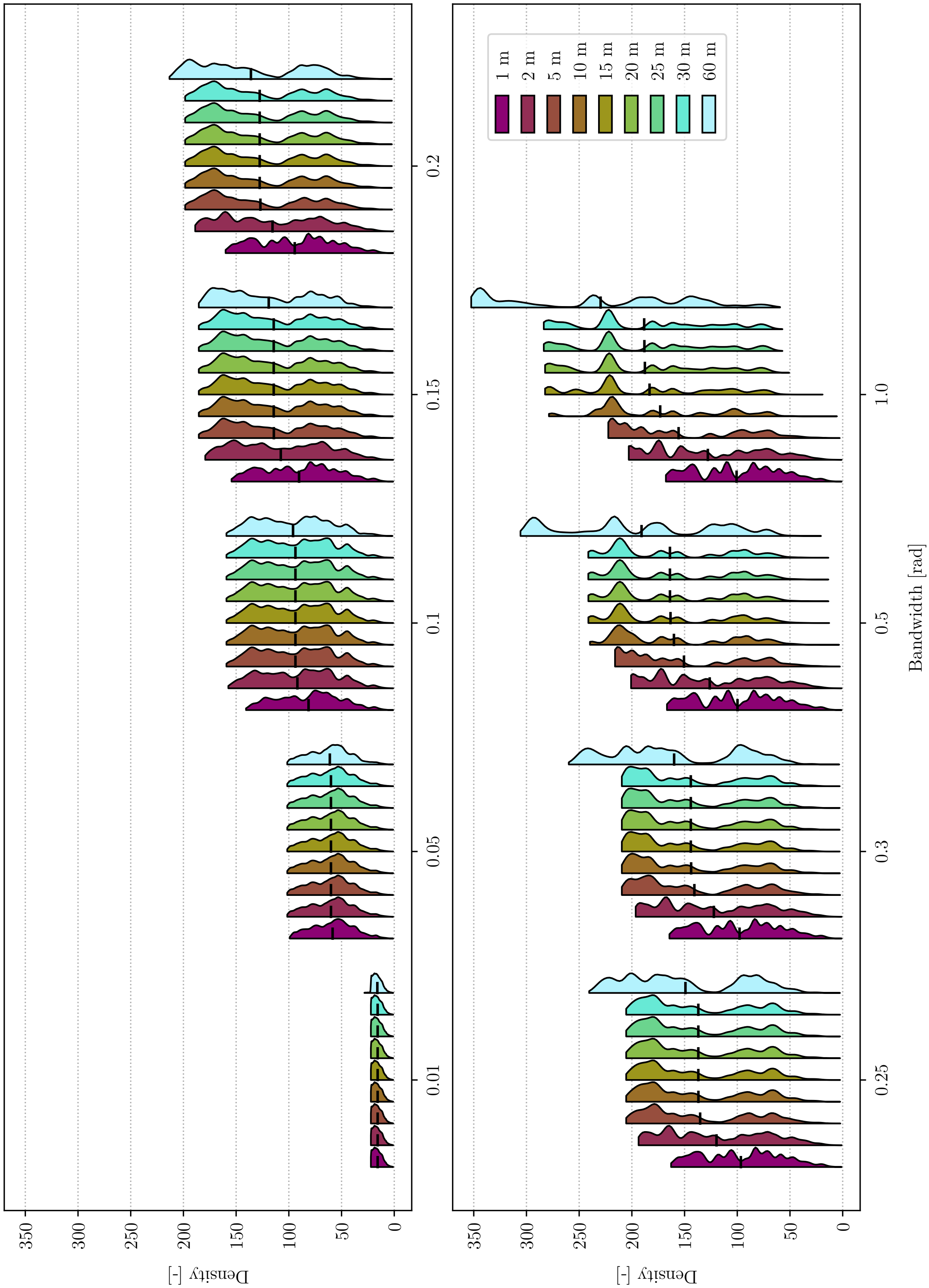

Figure S4. Violin plot of calculated densities from the Kernel Density Estimation sensitivity test. The 60-min time window grows considerably over the shorter windows due to counting multiple orbits in the same locality, especially when the bandwidth is large enough to consider further observations.

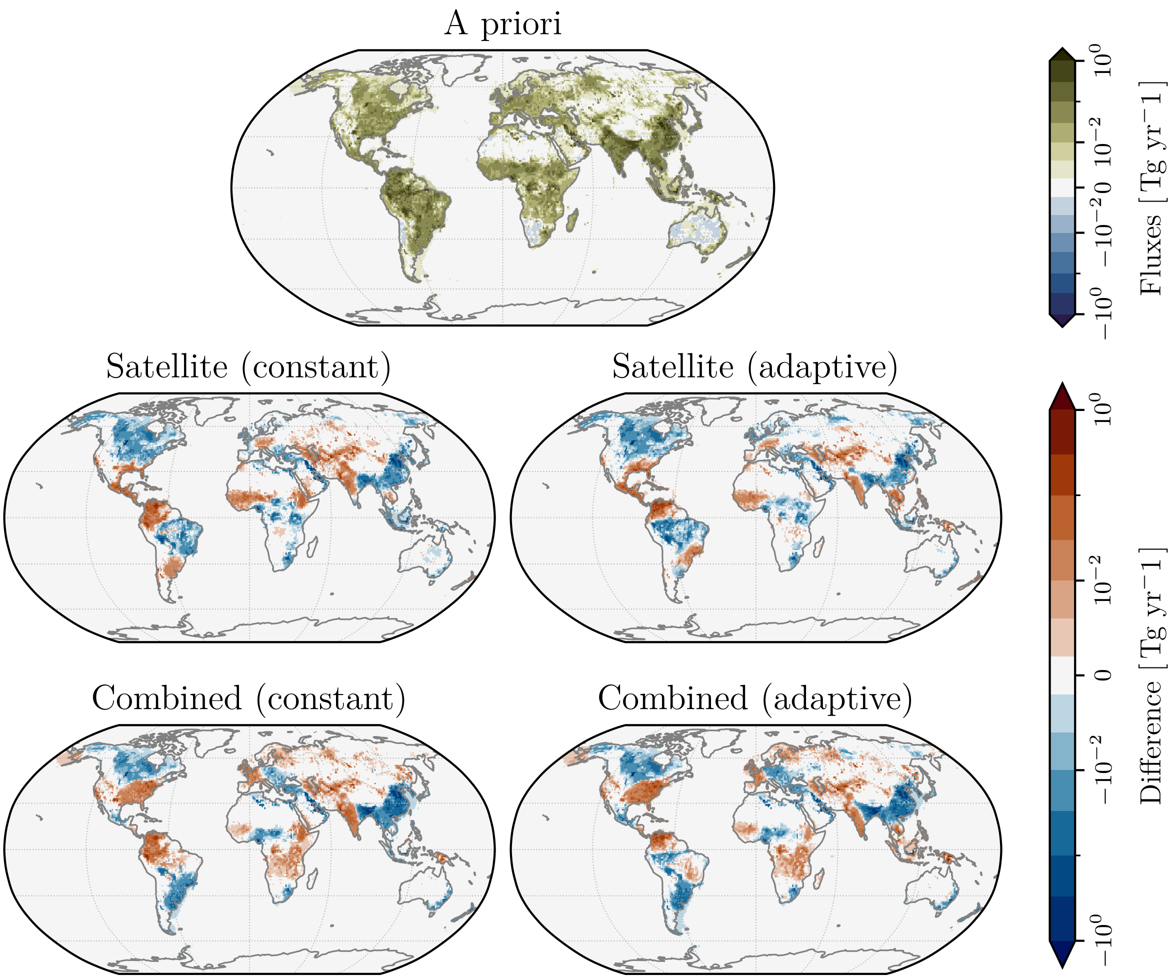

Figure S5. Change in annual total CH_4 fluxes for each inversion assimilating satellite data. The top pane shows the total a priori emissions as reference, below that the differences in posterior to those prior emissions for the four experiments that included satellite observations are shown (i.e., S2, S3, S4, and S5).

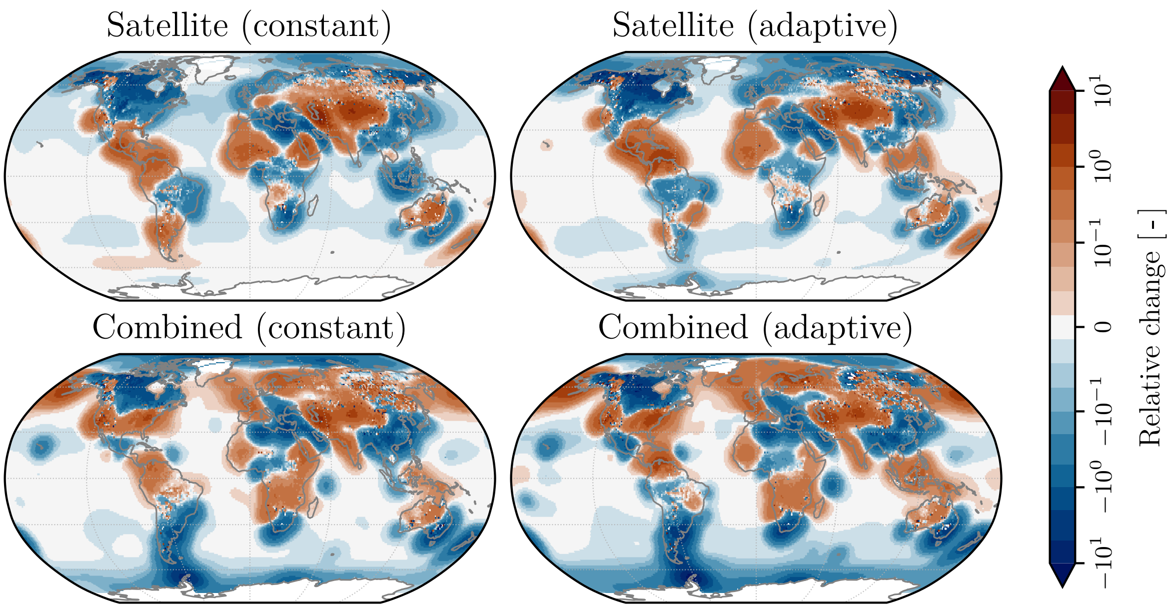

Figure S6. Symmetric relative change of total annual fluxes after optimization, calculated as the logarithm of the ratio of posterior over prior emissions.

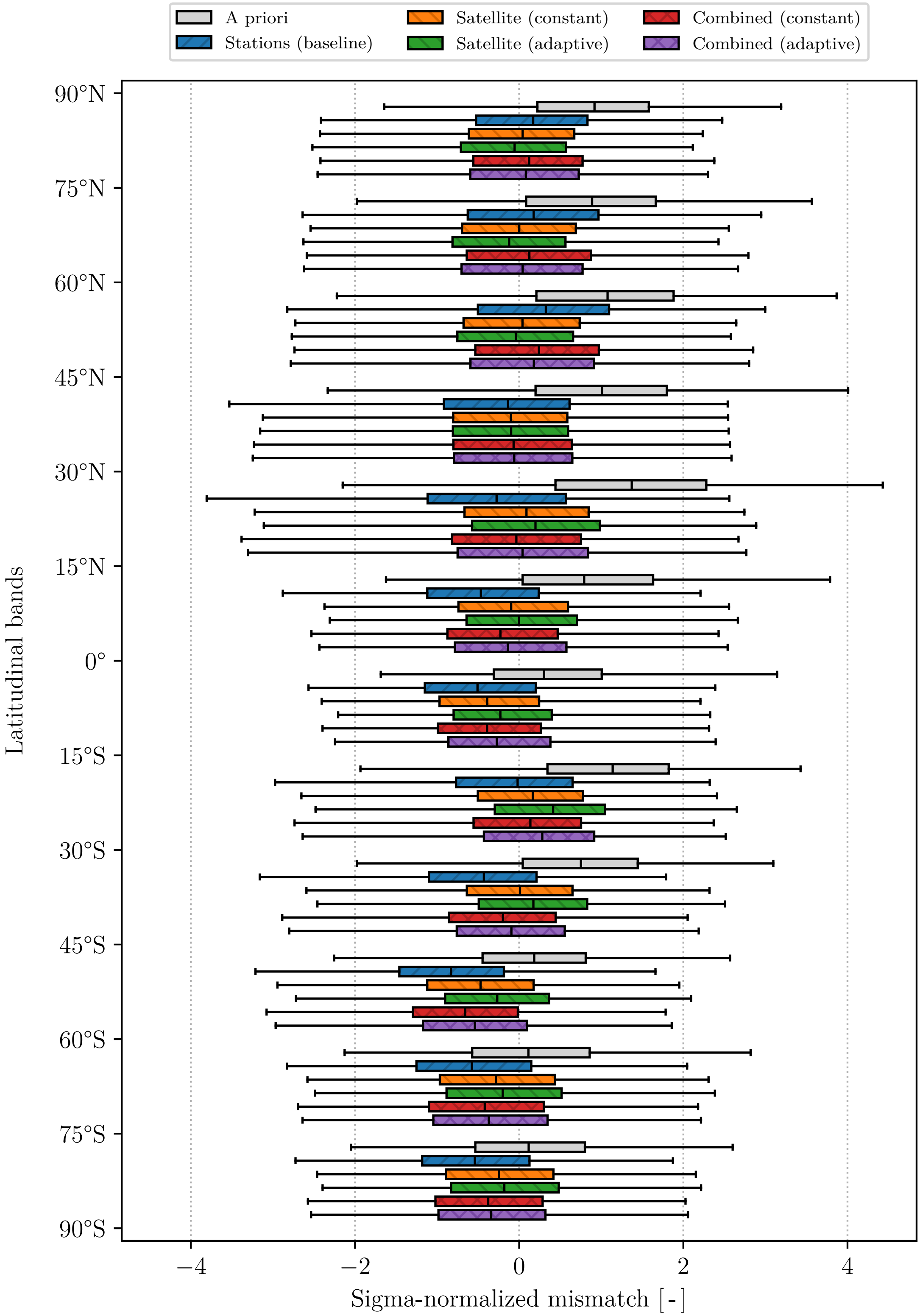

Figure S7. Sigma-normalized mismatch between columns simulated from optimized emissions and TROPOMI observations for 2019, averaged per latitudinal band. Whiskers show the 1st and 99th percentiles respectively, excluding outliers; boxes show the 25th and 75th percentiles, calculated using a single-pass stream *t*-digest algorithm (Dunning, 2021).

Table S4. Weighted RMSE for modeled columns against TROPOMI observations. Separated by latitudinal bands, hemisphere and global. Note that both the satellite-only and the combined inversions assimilate these data.

	A priori	Stations (baseline)	Satellite (constant)	Satellite (adaptive)	Combined (constant)	Combined (adaptive)
Latitudinal band						
(75°N, 90°N)	21.33	16.35	15.35	15.31	15.95	15.76
(60°N, 75°N)	21.11	17.56	15.49	15.48	16.71	16.29
(45°N, 60°N)	21.18	16.51	14.71	14.67	15.62	15.51
(30°N, 45°N)	18.47	14.28	13.17	13.27	13.49	13.52
(15°N, 30°N)	19.67	14.15	12.52	12.77	12.89	12.92
(0°, 15°N)	16.84	13.71	12.30	12.30	12.61	12.47
(15°S, 0°)	14.28	15.12	13.55	12.76	13.85	13.24
(30°S, 15°S)	16.91	12.58	11.64	12.39	11.82	12.14
(45°S, 30°S)	14.81	13.45	11.92	12.15	12.39	12.26
(60°S, 45°S)	13.51	17.00	14.89	13.78	15.85	15.05
(75°S, 60°S)	17.69	19.31	17.73	17.44	18.31	18.00
(90°S, 75°S)	16.64	18.39	16.75	16.54	17.32	17.10
Hemisphere						
Northern	19.44	14.84	13.34	13.45	13.86	13.81
Southern	16.40	15.41	14.06	14.15	14.45	14.36
Global	18.33	15.07	13.62	13.73	14.09	14.02

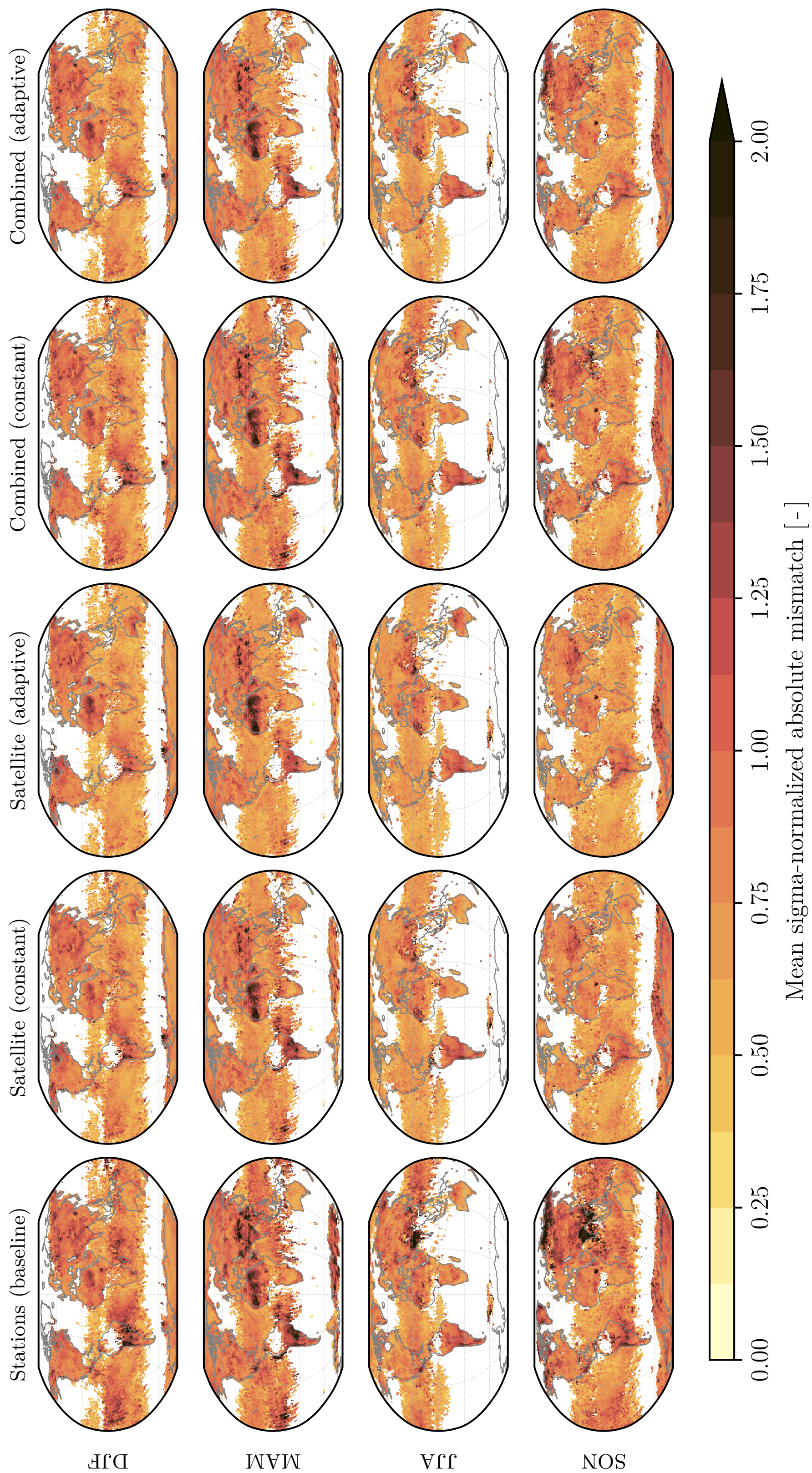

Figure S8. Mean absolute sigma-normalized mismatch between simulated columns from optimized emissions and TROPOMI observations, binned into model grid cells. Each row shows the seasonal mean for the analyzed year.

References

Buschmann, M., Petri, C., Palm, M., Warneke, T., and Notholt, J.: TCCON data from Ny-Ålesund, Svalbard (NO), Release GGG2020.R0, https://doi.org/10.14291/TCCON.GGG2020.nyalesund01.R0, 2022.

De Mazière, M., Sha, M. K., Desmet, F., Hermans, C., Scolas, F., Kumps, N., Zhou, M., Metzger, J.-M., Duflot, V., and Cammas, J.-P.: TCCON data from Réunion Island (RE), Release GGG2020.R0, https://doi.org/10.14291/TCCON.GGG2020.reunion01.R0, 2022.

Deutscher, N. M., Griffith, D. W., Paton-Walsh, C., Jones, N. B., Velazco, V. A., Wilson, S. R., Macatangay, R. C., Kettlewell, G. C., Buchholz, R. R., Riggenbach, M. O., Bukosa, B., John, S. S., Walker, B. T., and Nawaz, H.: TCCON data from Wollongong (AU), Release GGG2020.R0, https://doi.org/10.14291/TCCON.GGG2020.wollongong01.R0, 2023a.

Deutscher, N. M., Griffith, D. W., Paton-Walsh, C., Velazco, V. A., Wennberg, P. O., Blavier, J.-F., Washenfelder, R. A., Yavin, Y., Keppel-Aleks, G., Toon, G. C., Jones, N. B., Kettlewell, G. C., Connor, B. J., Macatangay, R. C., Wunch, D., Roehl, C., and Bryant, G. W.: TCCON data from Darwin (AU), Release GGG2020.R0, https://doi.org/10.14291/TCCON.GGG2020.darwin01.R0, 2023b.

Dunning, T.: The t-digest: Efficient estimates of distributions, Software Impacts, 7, https://doi.org/10.1016/j.simpa.2020.100049, 2021.

García, O. E., Schneider, M., Herkommer, B., Gross, J., Hase, F., Blumenstock, T., and Sepúlveda, E.: TCCON data from Izana (ES), Release GGG2020.R1, https://doi.org/10.14291/TCCON.GGG2020.izana01.R1, 2022.

Hase, F., Herkommer, B., Groß, J., Blumenstock, T., Kiel, M., and Dohe, S.: TCCON data from Karlsruhe (DE), Release GGG2020.R2, https://doi.org/10.14291/TCCON.GGG2020.karlsruhe01.R2, 2024.

Iraci, L. T., Podolske, J. R., Roehl, C., Wennberg, P. O., Blavier, J.-F., Allen, N., Wunch, D., and Osterman, G. B.: TCCON data from Edwards (US), Release GGG2020.R0, https://doi.org/10.14291/TCCON.GGG2020.edwards01.R0, 2022.

Kivi, R., Heikkinen, P., and Kyrö, E.: TCCON data from Sodankylä (FI), Release GGG2020.R0, https://doi.org/10.14291/TCCON.GGG2020.sodankyla01.R0, 2022.

Liu, C., Wang, W., Sun, Y., and Shan, C.: TCCON data from Hefei (PRC), Release GGG2020.R1, https://doi.org/10.14291/TCCON.GGG2020.hefei01.R1, 2023.

Morino, I., Ohyama, H., Hori, A., and Ikegami, H.: TCCON data from Rikubetsu (JP), Release GGG2020.R0, https://doi.org/10.14291/TCCON.GGG2020.rikubestsu01.R0, 2022a.

Morino, I., Ohyama, H., Hori, A., and Ikegami, H.: TCCON data from Tsukuba (JP), Release GGG2020.R0, https://doi.org/10.14291/TCCON.GGG2020.tsukuba02.R0, 2022b.

Morino, I., Velazco, V. A., Hori, A., Uchino, O., and Griffith, D. W.: TCCON data from Burgos, Ilocos Norte (PH), Release GGG2020.R0, https://doi.org/10.14291/TCCON.GGG2020.burgos01.R0, 2022c.

Notholt, J., Petri, C., Warneke, T., and Buschmann, M.: TCCON data from Bremen (DE), Release GGG2020.R0, https://doi.org/10.14291/TCCON.GGG2020.bremen01.R0, 2022.

Petri, C., Vrekoussis, M., Rousogenous, C., Warneke, T., Sciare, J., and Notholt, J.: TCCON data from Nicosia (CY), Release GGG2020.R1, https://doi.org/10.14291/TCCON.GGG2020.nicosia01.R1, 2024.

Pollard, D. F., Robinson, J., and Shiona, H.: TCCON data from Lauder (NZ), Release GGG2020.R0, https://doi.org/10.14291/TCCON.GGG2020.lauder03.R0, 2022.

Shiomi, K., Kawakami, S., Ohyama, H., Arai, K., Okumura, H., Ikegami, H., and Usami, M.: TCCON data from Saga (JP), Release GGG2020.R0, https://doi.org/10.14291/TCCON.GGG2020.saga01.R0, 2022.

Strong, K., Roche, S., Franklin, J. E., Mendonca, J., Lutsch, E., Weaver, D., Fogal, P. F., Drummond, J. R., Batchelor, R., Lindenmaier, R., and McGee, E.: TCCON data from Eureka (CA), Release GGG2020.R0, https://doi.org/10.14291/TCCON.GGG2020.eureka01.R0, 2022.

Sussmann, R. and Rettinger, M.: TCCON data from Garmisch (DE), Release GGG2020.R0, https://doi.org/10.14291/TCCON.GGG2020.garmisch01.R0, 2023.

Té, Y., Jeseck, P., and Janssen, C.: TCCON data from Paris (FR), Release GGG2020.R0, https://doi.org/10.14291/TCCON.GGG2020.paris01.R0, 2022.

Warneke, T., Petri, C., Notholt, J., and Buschmann, M.: TCCON data from Orléans (FR), Release GGG2020.R1, https://doi.org/10.14291/TCCON.GGG2020.orleans01.R1, 2024.

Wennberg, P. O., Roehl, C., Wunch, D., Blavier, J.-F., Toon, G. C., Allen, N. T., Treffers, R., and Laughner, J.: TCCON data from Caltech (US), Release GGG2020.R0, https://doi.org/10.14291/TCCON.GGG2020.pasadena01.R0, 2022a.

Wennberg, P. O., Roehl, C. M., Wunch, D., Toon, G. C., Blavier, J.-F., Washenfelder, R., Keppel-Aleks, G., and Allen, N. T.: TCCON data from Park Falls (US), Release GGG2020.R1, https://doi.org/10.14291/TCCON.GGG2020.parkfalls01.R1, 2022b.

Wennberg, P. O., Wunch, D., Roehl, C. M., Blavier, J.-F., Toon, G. C., and Allen, N. T.: TCCON data from Lamont (US), Release GGG2020.R0, https://doi.org/10.14291/TCCON.GGG2020.lamont01.R0, 2022c.

Wunch, D., Mendonca, J., Colebatch, O., Allen, N. T., Blavier, J.-F., Kunz, K., Roche, S., Hedelius, J., Neufeld, G., Springett, S., Worthy, D., Kessler, R., and Strong, K.: TCCON data from East Trout Lake, SK (CA), Release GGG2020.R0, https://doi.org/10.14291/TCCON.GGG2020.easttroutlake01.R0, 2022.

Zhou, M., Wang, P., Kumps, N., Hermans, C., and Nan, W.: TCCON data from Xianghe (CH), Release GGG2020.R0, https://doi.org/10.14291/TCCON.GGG2020.xianghe01.R0, 2022.